Proceedings of the 3rd World Congress on Momentum, Heat and Mass Transfer (MHMT'18)
Budapest, Hungary – April 12 - 14, 2018
Paper No. CSP 109
DOI: 10.11159/csp18.109

A Non-Adiabatic Flamelet Approach for Non-Premixed O2-CH4 Combustion

Paola Breda, Julian Zips, Michael Pfitzner
Universität der Bundeswehr München
85577 Neubiberg, Germany
paola.breda@unibw.de

Abstract **–** Numerical simulations of turbulent reactive flows are challenging due to the stiffness of chemical rate equations, depending on the number of species, reactions and time scales involved. A possible solution to speed-up the calculations is the use of tabulated manifolds for the thermo-chemical properties of the flame. In order to capture the effects of the flame-wall interactions, the pre-processed library shall include a parameter which accounts for heat losses. The generation of a non-adiabatic flamelet manifold is presented in this work, where the enthalpy defect experienced in proximity of the wall is included in the flamelet generation. A laminar simulation of a non-premixed methane/oxygen flame at elevated pressure is run to validate the manifold. The main differences to the frozen chemistry tabulation method previously in use are then underlined and referred to a finite rate chemistry case. Finally, a first assessment of the models was performed, based on a single-injector rocket chamber test case. The wall heat flux is compared with the available experimental results.

Keywords**:** Non-Adiabatic Flamelet, Flame-Wall Interaction, Non-Premixed Flame.

1. Introduction

Space exploration is driven by economic factors and relies on the performance of propellants. The propellant combination LOX/LH2 has been used successfully in liquid rocket engines because of its high specific impulse. However, the low specific gravity of liquid hydrogen requires bulky fuel tanks, meaning very large vehicle volumes. Methane as cryogenic hydrocarbon fuel looks promising as a candidate substitute to hydrogen [1] but still the combustion of CH4/O2 at high pressure is an open field of research. Higher chamber pressure leads to higher vehicle performance, which also turns into an increase of heat transfer. The numerical computation of heat loads and pressure distribution during the development phase of a rocket engine is therefore crucial, as design or material limits can be tracked and optimized for qualification and testing. Within the framework of SFB/TR 40 experimental results for a single-injector combustion chamber of gaseous methane and oxygen were provided [2] and will be used in this work.

A major drawback of a turbulent reactive flow simulation involving hydrocarbons is the high computational time, due to the number of species and reactions involved. A direct numerical simulation (DNS) with large hydrocarbons is unaffordable because of the chemical stiffness induced by highly reactive radicals and fast reversible reactions. Therefore, techniques aimed to reduce the chemistry mechanisms or modelling the chemistry-turbulence interaction are necessary. One possible way to remove the stiffness is by tabulating the thermo-chemical states during pre-processing, so that the CFD solver can look-up the values at run-time without solving the corresponding transport equations. In this work we based our method on the flamelet approach formulated by Peters [3], which separates the chemistry from the turbulence. Under the assumption that the chemistry time scales are fast compared to the flow scales, the turbulent flame can be reduced to a collection of thin laminar diffusion flames, whose thermo-properties can be tabulated in advance.

Yet the original model is not aware of heat losses, which can occur through radiation or near cooled walls, leading to a dropping of the reaction rates and promoting the recombination processes. The flame-wall interaction is a complex mechanism which should be taken into account when modelling the flame structure. The heat flux was discovered to influence the alignment of the flame towards the wall, with possible phenomena of head-on and side-wall flame quenching, as reported in [4] for premixed flames. A non-adiabatic correction shall be included as tabulation parameter, considering flame-radiation interaction [5], convective heat-loss [6] or modified thermal boundary conditions [7]-[8]. The latter work

introduces convective heat-loss effects to represent sidewall quenching and it was recently included in our in-house solver by Frank et al. [9].

The present study is focused on the generation of a non-adiabatic manifold based on the permeable-wall assumption [7], where the heat losses are recognized through an enthalpy defect parameter. Numerical models as well as the manifold generation are described in Section 2. The manifold is validated for a laminar flow simulation, whose results are reported in Section 3. The first results for a wall heat flux prediction in a turbulent simulation based on the single-injector combustion chamber are also described in Section 4. The conclusions and future work are drawn in Section 5.

2. Numerical Models

All simulations were parallelized and run with the OpenFOAM [10] framework, using a PISO algorithm for pressure correction. The 30-species skeletal mechanism from Lu and Law [11] was selected and it is referred to in the text as Lu30. Its validity for methane/oxygen counterflow diffusion flames at low strain rate was justified in a previous work [12]. Two tabulated combustion models were used as comparison, one based on frozen flamelets generated in Cantera [13], the other on non-adiabatic flamelets. Both manifolds were created at 20 bar with T_{CH4} = 269 K and T_{O2} = 278 K, the operative conditions of [2]. The frozen flamelet formulation was already presented by Frank [9] and the library was interpolated on 19 points in scalar dissipation rate χ and 1001 points in mixture fraction Z. In the next section we will focus on the non-adiabatic tabulation method. Preferential diffusivity was neglected by assigning unity Lewis numbers. Sutherland transport was chosen for OpenFOAM, with default coefficients for all species. The built-in mixture average model implementing the Wilke rule for the mixture viscosity was selected in Cantera.

2.1. Non-Adiabatic Flamelet Manifold

The flamelet structure in mixture fraction space is obtained by solving the flamelet equations

$$\rho \frac{\partial Y_k}{\partial t} - \frac{\rho\chi}{2}\frac{\partial^2 Y_k}{\partial Z^2} = \dot{\omega}_k \tag{1}$$

$$\rho \frac{\partial h_s}{\partial t} - \frac{\rho\chi}{2}\frac{\partial^2 h_s}{\partial Z^2} = -\sum_{k=1}^{n} h_k \dot{\omega}_k \tag{2}$$

where ρ is the density, χ the scalar dissipation rate, Z the mixture fraction. Given a species *k*, its mass fraction, standard enthalpy of formation and production rate are respectively Y_k, h_k and $\dot{\omega}_k$. The mixing process of the flame is controlled by the scalar dissipation rate, which in this case is assigned as a small value. The energy equation is solved for the sensible enthalpy h_s. The equations are closed with the reaction mechanism Lu30 and the ideal gas equation of state.

Fig. 1 shows the extension of the theory to include non-adiabatic effects. A permeable, inert wall is inserted at Z_{wall} and allows only mass diffusion towards the right hand side of the domain. In the original formulation the source terms of Eq. (1) and the temperature equation were set to zero for $Z_{wall} < Z < 1$ [8]. Here the flame temperature is linearly interpolated between T_{wall} and T_{fuel}. The adiabatic counterflow diffusion flame is solved in the first place, with the wall located in Z = 1 and $T_{wall} = T_{fuel}$. Afterwards the wall is shifted from Z = 1 towards the flame front and T_{wall} decreased by 3K at each step, until flame quenching is reached. The temperature profiles before quenching are shown in Fig. 2. Strain effects are not taken into account.

The laminar flamelet library is generated as a function of the mixture fraction and the normalized enthalpy, defined as

$$h_{norm} = \frac{h - h_{min}}{h_{max} - h_{min}} \tag{3}$$

with h_{max} taken from the adiabatic flame, h_{min} from the last calculated flamelet before quenching and *h* is the flamelet absolute enthalpy. The manifold is discretized on 50 points in h_{norm} and 202 points in Z.

The dashed lines in Fig. 3 show the boundaries for h_{min} in black and h_{max} in red. By closer observation an intersection of the enthalpy profiles can be detected in the range $0.8 < Z < 1$, after the curves reach their minimum at the permeable wall. This was already observed for the temperature profiles in [8]. The h_{max} profile is also intersected by the non-adiabatic flamelets, leading to a difficult selection of the upper and lower boundaries.

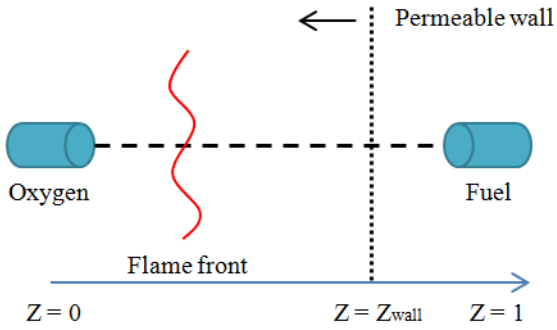

Fig. 1: Counterflow diffusion flame with inert permeable wall.

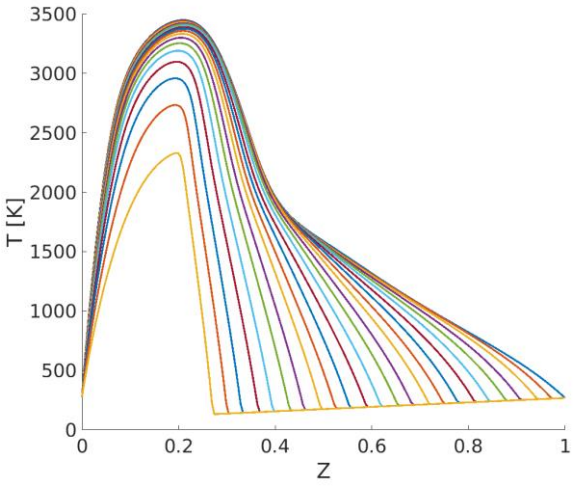

Fig. 2: Non-adiabatic flamelet solution for $\chi = 10\ s^{-1}$.

The manifold was then extended beyond its boundaries using the frozen chemistry assumption. The mixture composition of the adiabatic flamelet was kept constant while increasing the enthalpy. The last flamelet before quenching was also cooled down with frozen composition. In Fig. 3 the final manifold with one extension beyond h_{max} and twenty towards h_{min} is also shown. Finally the manifold can be imported in OpenFOAM and used for the laminar simulations, where the thermo-chemical states can be retrieved by means of the parameters (Z, h_{norm}).

2.2. Turbulence Model

The hybrid LES-RANS improved version from the DDES model [14] was chosen for the turbulent simulation. Two additional filtered transport equations are required for the mean mixture fraction $\tilde{Z}$ and its variance $\widetilde{Z''^2}$

$$\frac{\partial \bar{\rho}\tilde{Z}}{\partial t} + \frac{\partial \bar{\rho}\tilde{u}_j\tilde{Z}}{\partial x_j} = \frac{\partial}{\partial x_j}\left(\left(\frac{\bar{\mu}}{Sc} + \frac{\mu_{SGS}}{Sc_t}\right)\frac{\partial \tilde{Z}}{\partial x_j}\right) \tag{4}$$

$$\frac{\partial \bar{\rho}\widetilde{Z''^2}}{\partial t} + \frac{\partial \bar{\rho}\tilde{u}_j\widetilde{Z''^2}}{\partial x_j} = \frac{\partial}{\partial x_j}\left(\left(\frac{\bar{\mu}}{Sc} + \frac{\mu_{SGS}}{Sc_t}\right)\frac{\partial \widetilde{Z''^2}}{\partial x_j}\right) - 2\bar{\rho}\tilde{\chi} + 2\left(\frac{\bar{\mu}}{Sc} + \frac{\mu_{SGS}}{Sc_t}\right)\left(\frac{\partial \tilde{Z}}{\partial x_j}\right)^2 \quad (5)$$

with u_j the velocity vector and $Sc = Sc_t = 1$ the Schmidt numbers for the laminar and turbulent case. The bar $\bar{*}$ denotes the finite-volume filter, while the Favre-filtering is marked as $\tilde{*}$. The diffusive term consist of a molecular viscosity μ and a subgrid viscosity μ_{SGS}, the last modelled according to Smagorisky. The additional equation for the near-wall resolution is taken from Spalart and Allmaras [15] for the RANS model.

To extend the applicability of the manifold to a turbulent solver, the mean values for species mass fraction and temperature are calculated by means of a presumed probability density function (PDF). The PDF shape for the enthalpy is modeled with a Dirac function centered in $\tilde{h}_{norm}$, whereas the mixture fraction is approximated using a presumed β-PDF. The turbulent CFD solver will look-up the species mass fractions and temperature as a function of $(\tilde{Z}, \widetilde{Z''}, \tilde{h}_{norm})$. The β-PDF integration for the mixture fraction variance is done on 10 points for each flamelet library.

3. Laminar Diffusion Flame

A finite rate chemistry simulation with the skeleton mechanism Lu30 is used as reference case for the tabulation methods. The selected 2D geometry is presented in Fig. 4 and it resembles the operative conditions of the combustion chamber used for the turbulent case. Methane and oxygen are injected at respectively 269 K and 278 K with a velocity of 1 m/s, separated by a wall tip of 5 mm. The wall temperature T_{wall} = 380K was chosen as the average of the experimental values at wall in the domain. Final results are presented for a fine grid of about $1.6 \cdot 10^5$ cells.

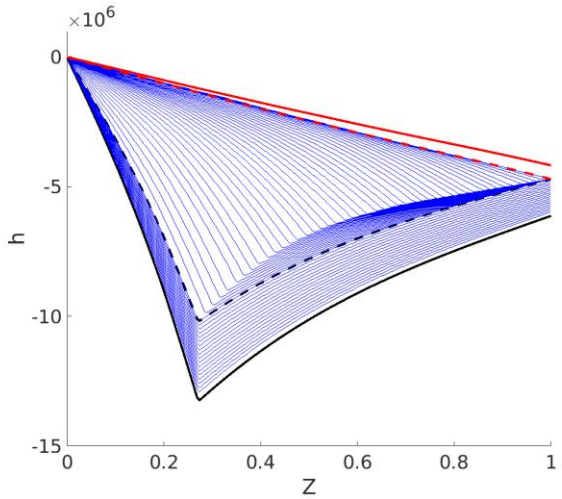

Fig.3: Absolute enthalpy space: h_{min} in black and h_{max} in red. Dashed lines delimit the original manifold, full lines the final one with the frozen chemistry correction.

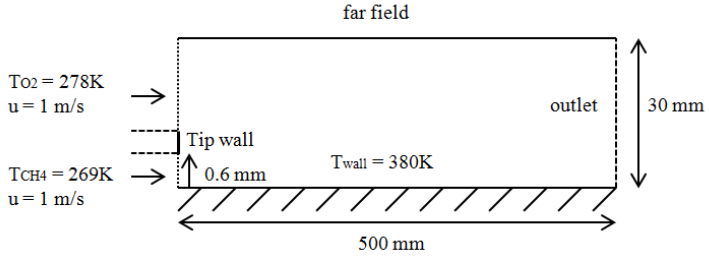

Fig. 4: 2D computational domain for the laminar case. Not in scale.

3.1. Results

The right plot in Fig. 5 shows the wall heat flux distribution of the non-adiabatic flamelet method compared to the frozen chemistry and the finite rate solution. The domain can be split into two regions at the coordinate x = 0.3m. The first region is fuel-rich and is still better represented by the frozen set. The left plot shows that the production of H_2O is underestimated in the Wu flamelet close to the inlet, which might cause the under prediction of heat release in the first part. Since $T_{wall} > T_{fuel}$ a positive peak at inlet is visible due to the heating of CH_4. In the second region the non-adiabatic flamelets better approximate the finite rate solution. Here the frozen flamelets underestimate the wall heat flux because CO is consumed slower and the concentration of CO_2 is nearly unchanged.

Fig. 6 shows two wall-normal sections for the fuel-rich region. The first row is the integrated heat of reaction, which shows how the non-adiabatic set better agrees with the finite rate solution far from the injector plate. The first peak at r~2.5mm corresponds to the endothermic reaction of CH_4 with high production of CO and H_2 as shown in the bottom plots. Their production is still slightly over predicted by both methods. The heat spike indeed is well captured by the non-adiabatic set at x = 0.2 mm.

The second peak at r ~ 3.5mm captures the recombination of H_2 and OH into H_2O and locates the flame position. The peak location for the non-adiabatic flamelets coincides with the finite rate case but its value is lower. The water prediction is in good agreement. The final peak for the recombination of CO into CO_2 at r~6mm is overestimated by the non-adiabatic set. Since the chemical species are not transported and their source term is not integrated in the solver, one possible source of error can be found in the total heat release of the original libraries.

The bottom right figure shows the radicals OH and O confined in the reaction zone and not present at wall. There is a non-adiabatic effect captured by the non-null derivative of species H_2 and CO at wall. Eq.(1) shows that the only term which can introduce concentration variation at wall is the diffusion of species, in case radicals recombination reactions are present at wall.

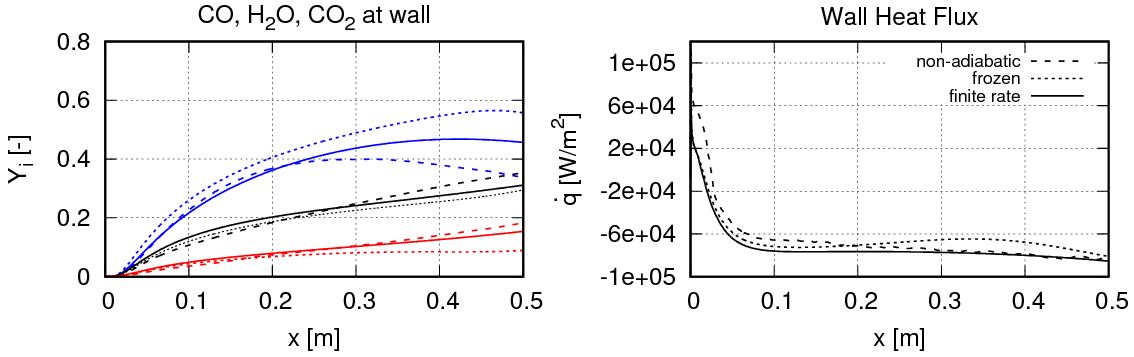

Fig. 5: CO (blue), H_2O (black) and CO_2 (red) mass fractions and heat flux at wall along the axis, for non-adiabatic flamelets, frozen chemistry and finite rate solution.

4. Turbulent Flame

Preliminary results are discussed for a turbulent flame. The test case is the single-injector combustion chamber operated at 20bar and reported in details in [16], with a squared cross section of 12 x 12 mm^2. GOX and GCH4 are injected via a coaxial injector at respectively 278K and 269K, with mass flow rates of 45 g/s and 17 g/s. Since the flamelets will be further validated in a configuration with film cooling [17] the computational domain was shortened from the original 303mm to 150mm, in order to investigate the near-injector region. Temperature distributions are available from thermocouples readings, which allow for a comparison of the wall heat flux.

4.1. Numerical Setup

The coaxial injector is not included in the CFD domain, but LES inlet boundary conditions based on the digital filter approach [18] guarantee for inflow turbulence. The wall temperature is assigned and interpolated on the wall patches from

experimental measurements. Faceplate and posttip are considered adiabatic. Pressure is relaxing towards $1.87 \cdot 10^6$ Pa at outlet. A structured mesh was discretized with 10 cells at the posttip to catch the flame structure. The posttip cells are refined to 50µm for the first 50cm along the axis, 200µm elsewhere. A cell size of 0.2µm at wall guarantees for $y^+ < 1$. The spatial discretization is a 2nd order central difference scheme of type TVD with van Leer limiter. The time discretization method is implicit Euler, with a maximum global CFL of 0.4.

4.2. Flow Features

A coarse mesh with 6 cells at the posttip was first used to catch the mean flow features, averaged over 1 ms. Fig. 7 shows the mean CH_4 field, the upper side of the chamber being the frozen chemistry solution, the bottom the non-adiabatic one. After the recirculation zone a thick reaction zone can be seen until 50mm, it extends longer in the non-adiabatic case. The mean temperature field in Fig. 8 is slightly colder in the frozen case although a colder layer at wall is present in the non-adiabatic case.

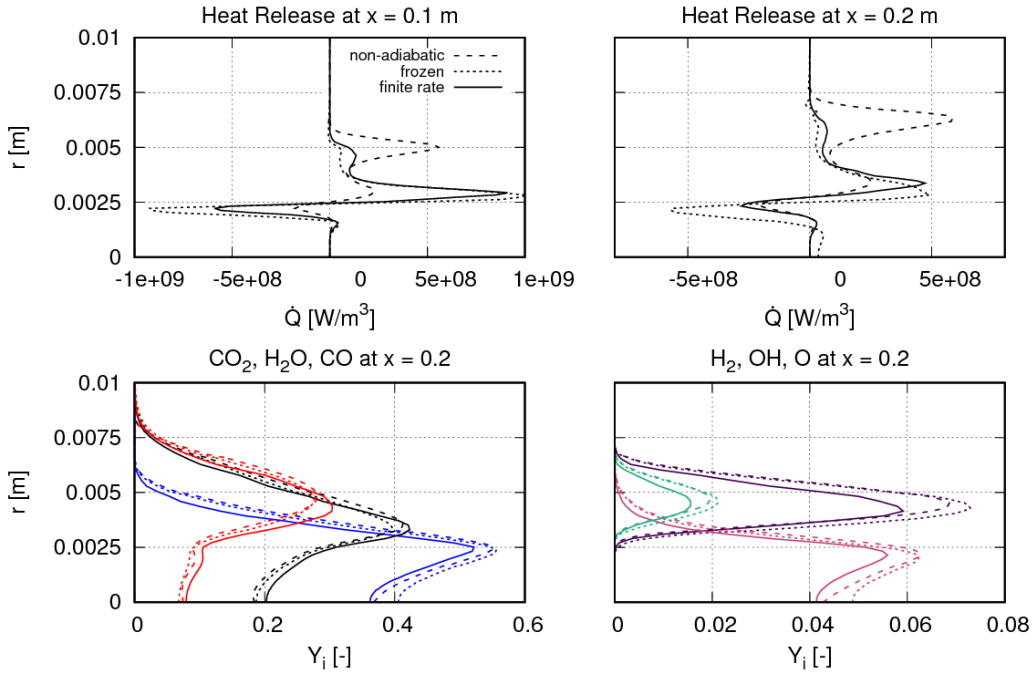

Fig. 6: In the first row, wall-normal plots for combustion heat release at x = 0.1m and 0.2m respectively. In the second row the major products at x = 0.2m.: CO (blue), H_2 (black), CO_2 (red). H_2 (magenta), OH (purple), O (green).

Along the walls also a thin layer of colder methane is visible. As CH_4 recirculates at the corners of the combustion chamber closed to the faceplate, the wall heat flux circumferential distribution will not be homogeneous due to the squared cross-section. Overall the two methods generate more similar field distributions, compared to the previous configuration in laminar regime.

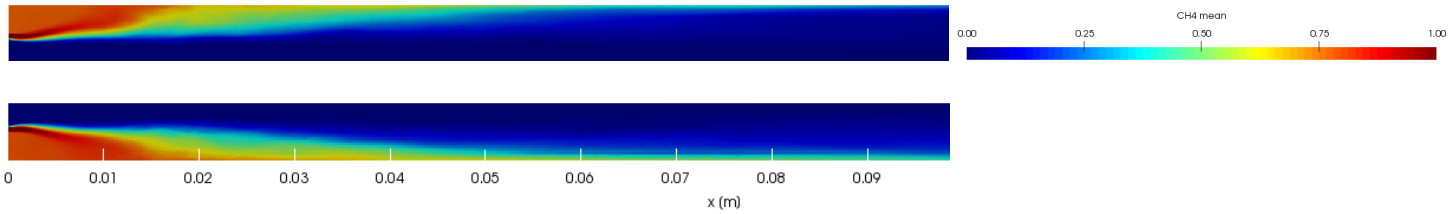

Fig. 7: CH_4 mean field. Upper half: frozen flamelets manifold. Bottom half: non-adiabatic flamelets.

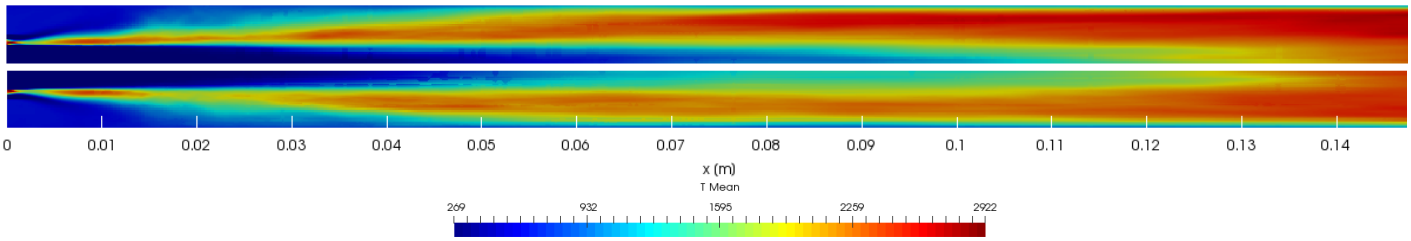

Fig. 8: Temperature mean field. Upper half: frozen flamelets manifold. Bottom half: non-adiabatic flamelets.

Fig. 9 shows the local temperature field for the coarse and the fine mesh in the non-adiabatic simulation. The recirculation zone at the face plate is visible and it extends to about 20 cm in the chamber. The Kelvin-Helmoltz vortices can be also seen in the first 10 cm where the flame expands. The flame is higher strained in the fine grid, except in the region close to the injector, where it is thinner in the coarse mesh. The maximal temperature reached is circa 3450K which is close to the adiabatic flame temperature for O2 and CH4 under such conditions, 3444K.

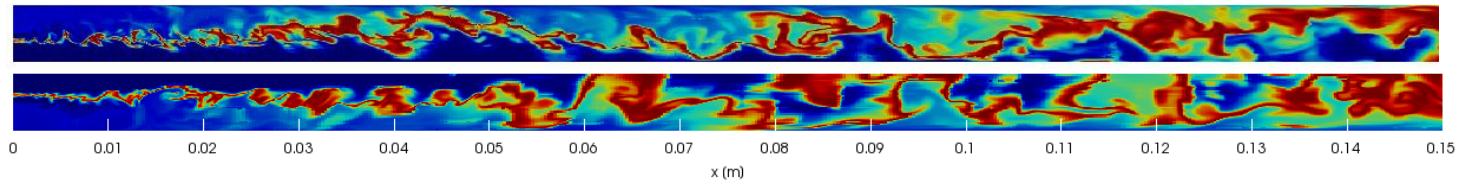

Fig. 9: Local temperature fields. Top: fine mesh. Bottom: coarse mesh.

4.3. Comparison with the Experiment

A final comparison for the wall heat flux for the fine mesh is shown in Fig. 10. The wall heat flux is an important design parameter for rocket engines and it is evaluated in the solver from the temperature gradient and thermal diffusivity. A circumferential average was necessary due to the squared cross-section.

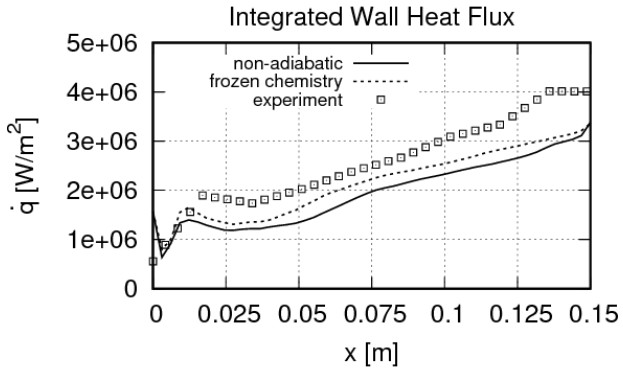

Fig. 10: Wall heat flux at wall. Tabulated methods compared with the experimental results.

Both flamelet manifolds under estimate the experimental values. The peak around 15mm occurs at the end of the recirculation zone where the hot gas impacts against the wall. In the central zone the heat flux from the experiment increases linearly along the axis, whose behaviour is not represented by the two manifolds. Both profiles show a non-linear increase in heat flux at half of the chamber, with the frozen chemistry solution approaching the experimental results. In the near-injector zone and at outlet the methods better agree. The frozen chemistry predicts a better mixing and fuel consumption but results in higher mean chamber pressures.

5. Conclusion

An extension of the original non-adiabatic flamelet model with permeable wall was presented, where mixture fraction and normalized enthalpy were chosen as look-up parameters. The manifold was then tested in a laminar and a turbulent case. The laminar case revealed a good prediction of the heat flux in the second part of the domain, the frozen set approximates better the fuel-rich zone. The two methods could therefore be coupled to be separately selected only in the interested zones. The turbulent case instead revealed an under estimation of the wall heat flux, with the methods in agreement at inlet and outlet. The turbulent simulations will be taken as reference case for a future investigation on non-reacting film cooling.

The non-adiabatic tabulation method can be rethought with temperature as lookup parameter instead of enthalpy. This could further smooth the temperature oscillations at wall and give a better wall heat flux prediction. The fact that the CH_4-rich side of a diffusion flame is affected by higher strain rates also suggests the introduction of χ as fourth tabulation parameter to improve accuracy.

References

[1] G. P. Sutton and O. Biblarz, *Rocket Propulsion Elements*. John Wiley & Sons, New York, 8th ed. 2010.

[2] M. P. Celano, S. Silvestri, G. Schlieben, C. Kirchberger, O. J. Haidn and S. Menon, "Injector Characterization for a Gaseous Oxygen-Methane Single Element Combustion Chamber," in *Progress in Propulsion and Power*, vol. 8, 2016, pp. 145-164.

[3] N. Peters, "Laminar diffusion flamelet models in non-premixed turbulent combustion," in *Progress in Energy Combustion Science*, vol. 10, no. 3, 1984, pp. 319-339.

[4] Dreizler and B. Böhm, "Advanced laser diagnostics for an improved understanding of premixed flame-wall interactions," in *Proc. Combust.Inst.*, vol. 35, 2015, pp. 37-64.

[5] M. Hossain, J. C. Jones and W. Malalasekera, "Modelling of a bluff-body nonpremixed flame using a coupled radiation/flamelet combustion model," in *Flow, Turb. Combustion*, vol. 67, no. 3, pp. 217-234, 2001.

[6] D. J. Lee, S. Thakur, J. Wright, M. Ihme and W. Shyy, "Characterization of Flow Field Structure and Species Composition in a Shear Coaxial Rocket GH2/GO2 Injector: Modelling of Wall Heat Losses," in *AIAA 2011-6125*, San Diego, CA.

[7] H. Wu and M. Ihme, "Modelling of Wall Heat Transfer and Flame/Wall Interaction A Flamelet Model with Heat-Loss Effects," in *9th U.S. National Combustion Meeting*, Cincinnati, Ohio, 2015.

[8] P. C. Ma, H. Wu, M, Ihme and J. P. Hickey, "A flamelet model with heat-loss effects for predicting wall-heat transfer in rocket engines," in *Propulsion and Energy Forum*, Atlanta, GA, 2017.

[9] G. Frank, J. Zips, M. Pfitzner, "Construction of Libraries for Non-Premixed Tabulated Chemistry Combustion Models including Non-Adiabatic Behaviours due to Wall Heat Losses," in *Sonderforschungsbereich/Transregio 40 Annual Report*, 2014.

[10] H. G. Weller, G. Tabor, H. Jasak and C. Fureby, "A tensorial approach to computational continuum mechanics using object-oriented techniques," in *Computers in Physics*, vol. 12, no. 6, 1998.

[11] T. F. Lu and C. K. Law, "A criterion based on computational singular perturbation for the identification of quasi steady state species: A reduced mechanism for methane oxidation with NO chemistry," *Combustion and Flame*. vol. 154, no. 4, 2008, pp. 761-774.

[12] M. Hansinger, P. Breda, J. Zips and M. Pfitzner, "Hybrid RANS/LES simulation of a GOX/GCH4 7-element rocket combustor using a non-.adiabatic flamelet method," in *Sonderforschungsbereich/Transregio 40 Annual Report*, 2017.

[13] Cantera, Cerfacs. [Online]. Available: http://www.cerfacs.fr/cantera/description.php

[14] M. L. Shur, P. R. Spalart, M. K. Strelets and A. K. Travin, "A hybrid RANS-LES approach with delayed-DES and wall-modelled LES capabilities," in *International Journal of Heat and Fluid Flow*, vol. 26, no. 6, pp. 1638-1649, 2008.

[15] P. Spalart and S. Allmaras, "A one-equation turbulence model for aerodynamic flows," in *La Rech. Aeropatiale*, vol. 1, no. 1, pp. 5-21, 1994.

[16] O. Haidn, M. P. Celano, S. Silvestri, G. Schlieben, C. Kirchberger, *Test Case 1: Single Element Combustion Chamber – GCH4-GOX. Transregio Test Case 1*. 2015.
[17] M. P. Celano, S. Silvestri, C. Kirchberger , G. Schlieben, D. I. Suslov, O. J. Haidn, "Gaseous Film Cooling Investigation in a Model Single Element GCH4-GOX Combustion Chamber," in *Trans. JSASS Aerospace Tech. Japan*, vol. 14, no. Ists30, pp. 129-137, 2016.
[18] M. C. Immer, "Time-resolved measurement and simulation of local scale turbulent urban flow," Ph.D. dissertation, ETH Zürich, 2016.